
ENGINEERING SOFTWARE 2.0 BY INTERPOLATING NEURAL NETWORKS: UNIFYING TRAINING, SOLVING, AND CALIBRATION

Chanwook Park *

Department of Mechanical Engineering
Northwestern University
Evanston, IL 60208
chanwookpark2024@u.northwestern.edu

Sourav Saha *

Kevin T. Crofton Department of
Aerospace and Ocean Engineering
Virginia Polytechnic Institute
and State University
Blacksburg, VA 24060
souravsaha@vt.edu

Jiachen Guo

Theoretical and Applied Mechanics Program
Northwestern University
Evanston, IL 60208
jiachenguo2020@u.northwestern.edu

Hantao Zhang

Theoretical and Applied Mechanics Program
Northwestern University
Evanston, IL 60208
hantaozhang2029@u.northwestern.edu

Xiaoyu Xie

Department of Mechanical Engineering
Northwestern University
Evanston, IL 60208
xiaoyuxie2020@u.northwestern.edu

Miguel A. Bessa

School of Engineering
Brown University
Providence, RI
miguel_bessa@brown.edu

Dong Qian

Department of Mechanical Engineering
University of Texas at Dallas
Richardson, TX 75080
dong.qian@utdallas.edu

Wei Chen

Department of Mechanical Engineering
Northwestern University
Evanston, IL 60208
weichen@northwestern.edu

Gregory J. Wagner

Department of Mechanical Engineering
Northwestern University
Evanston, IL 60208
gregory.wagner@northwestern.edu

Jian Cao

Department of Mechanical Engineering
Northwestern University
Evanston, IL 60208
jcao@northwestern.edu

Wing Kam Liu †

Department of Mechanical Engineering
Northwestern University
Evanston, IL 60208
w-liu@northwestern.edu

September 12, 2024

ABSTRACT

*Equal contribution with Coauthor 1 and Coauthor 2

†Corresponding author

The evolution of artificial intelligence (AI) and neural network theories has revolutionized the way software is programmed, shifting from a hard-coded series of codes, *Software 1.0*, to a vast neural network, *Software 2.0*. However, this transition in engineering software has faced challenges such as data scarcity, multi-modality of data, low model accuracy, and slow inference. Here, we propose a new network based on interpolation theories and tensor decomposition, the interpolating neural network (INN) to open the new era of *Engineering Software 2.0* that unifies training, solving, and calibration. Instead of interpolating training data, a common notion in computer science, INN interpolates grid points in the physical space whose coordinates and values are trainable. INN features orders of magnitude fewer trainable parameters (or degrees of freedom for solving), faster training/solving, less inference cost, smaller memory footprint, and higher model accuracy compared to multi-layer perceptron (MLP) or physics-informed neural networks (PINN). Various numerical experiments that cover computer science and engineering domains demonstrate that INN can solve over Zetta scale (10^{21}) partial differential equations and train/calibrate a dataset with extraordinary accuracy but fewer parameters using only a single graphics processing unit (GPU).

1 Introduction

The evolution of software programming methodologies has transitioned from reliance on rigidly hard-coded instructions, governed by explicitly defined human rules, to the adoption of neural network-based algorithms. The transition is coined as "from *Software 1.0* to *Software 2.0*" [1]. The shift towards *Software 2.0* has facilitated significant advancements in the domain of large language models (LLMs) and other foundational models [2, 3]. However, the application of these technologies within the field of engineering and science introduces distinct challenges. These challenges include scarcity and multi-modal aspect of data, low generalization error compared to classical numerical methods [4, 5, 6, 7], slow inference (function evaluation) time that challenges real-time control [8, 9, 10, 11] and statistical modeling, and resource-heavy model architecture [12, 13, 14, 15].

In this article, we propose the concept of *Engineering Software 2.0*, which aims to advance the current generation of computational and data-driven engineering software into a new paradigm.

"Engineering Software 2.0 is an end-to-end software system that unifies training, solving, and calibration in science/engineering problems."

As one promising enabler of *Engineering Software 2.0*, we introduce interpolating neural networks (INN). The key ideas behind INN are: 1) discretize an input domain into non-overlapping segments whose bounds are denoted by interpolation nodes, 2) construct a graph with the interpolation nodes and formulate the message-passing operation as a form of classical interpolation functions, and 3) optimize the values and coordinates of the interpolation nodes. Figure 1 shows the pictorial explanation of the approach. Note that one can also extrapolate for a certain range if the interpolation points are located outside of the range of training data. INN facilitates three major tasks in computational science and engineering: 1) train (or learn) on both experimental and simulation data with very high accuracy and minimal memory footprint, 2) solve high-dimensional partial differential equations (PDEs) with statistics involved, and 3) calibrate (or solve inverse problems) for uncertain parameters.

When the input domain is discretized with a regular mesh (see the special case of Figure 1), INN leverages the separation of variables and tensor decomposition (TD) [16, 17, 18, 19] to convert the growth rate of the computational cost of a high-dimensional problem from exponential to linear. This enables solving extremely challenging (over exascale, 10^{18}) high-dimensional PDEs or training data with hundreds of input variables within the interpolation framework.

Our results demonstrate that INN can markedly enhance training/inference speed and model accuracy compared to the multilayer perceptron (MLP) or physics-informed neural network (PINN)[20] by dramatically reducing the number of trainable parameters and network connectivity. This also results in a huge reduction in the usage of random-access memory (RAM) and disk storage, facilitating the transferability of a trained/solved model across multiple workstations. Furthermore, INN can adapt its network structure further to improve model accuracy or incorporate statistical behavior. INN has a huge potential of replacing MLP and convolutional neural network (CNN) [21] in modern AI models with the aforementioned benefits.

2 INN: Unifying Training/Learning, Solving, and Calibration

Interpolating Neural Network (INN) generalizes numerical methods such as finite element method (FEM) [22, 23, 24] and neural networks such as multi-layer perceptron (MLP) as a graph network operation. Although the two (i.e., numerical methods and neural networks) have been developed by seemingly different groups of researchers, they share

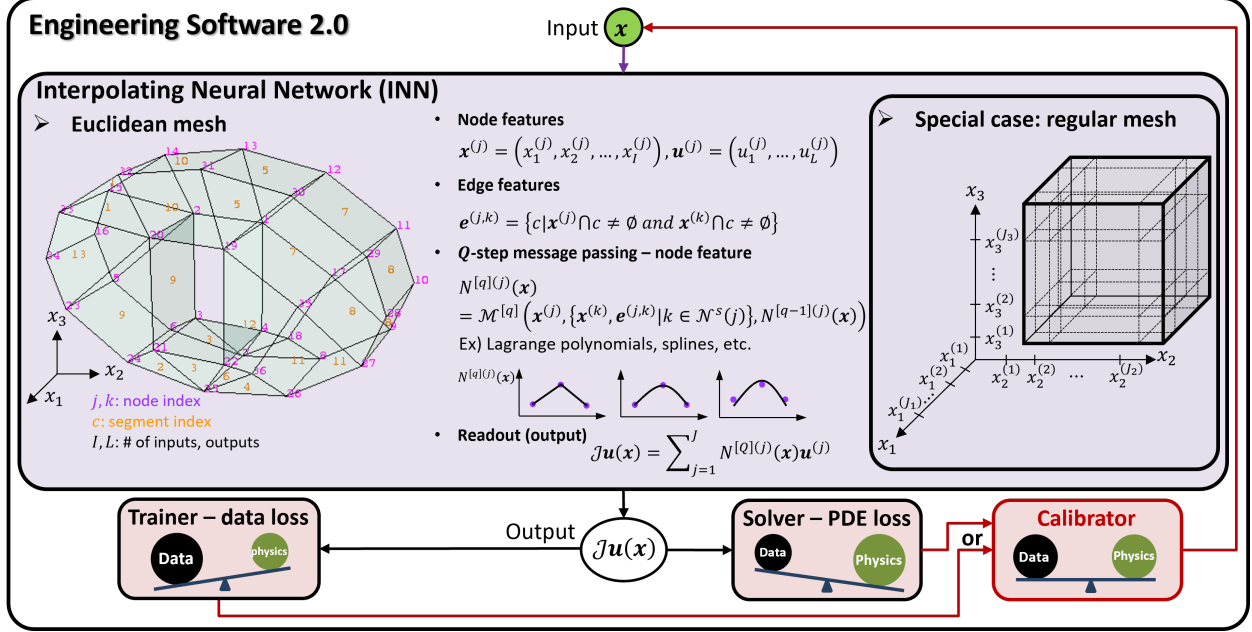


Figure 1: Overview of Engineering Software 2.0 enabled with Interpolating Neural Networks (INN). The INN box illustrates the graph representation of the input domain discretized with an arbitrary Euclidean mesh (left) and a regular mesh as a special case (right). Node and edge features are given from the discretized mesh. After Q -step message passing, each node j will store an interpolation function $N^{[Q](j)}(\mathbf{x})$. Finally, the readout operation sums the product of the interpolation functions and nodal values $\mathbf{u}^{(j)}$. The superscripts with square brackets $[\]$ and parentheses $(\)$ denote the message passing step and graph node index, respectively. The interpolation operator \mathcal{J} denotes that $\mathcal{J}\mathbf{u}(\mathbf{x})$ is a function that interpolates discrete values of $\mathbf{u}^{(j)}$. The INN trainer employs data-driven loss functions (e.g., mean squared error loss for regression) while the INN solver adopts a residual loss of a partial differential equation (PDE). A trained/solved INN model can then be employed as a forward model of a calibrator to solve an inverse problem.

one thing in common; the goal is to find a function. The former finds a solution field of a differential equation while the latter finds an input-output relationship. INN is built upon this similarity and forms the backbone of Engineering Software 2.0 that unifies training, solving, and calibration, as illustrated in Figure 1.

Consider a regression problem that relates I inputs and L outputs. The first step of INN is to discretize the input domain in the I -dimensional Euclidean space into a mesh, which can be as general as an unstructured irregular mesh or as specific as a structured regular mesh. In any case, a mesh in the Euclidean space can be readily represented as a graph – the most general form of a discretized input, as illustrated in the INN box of Figure 1. Note that this conversion from mesh to graph has been widely accepted in literature [25, 26, 27]. Suppose there are J nodes (or vertices) and E edges in the graph, where the input domain is discretized with C non-overlapping segments. Each node (e.g., node j) has two features: nodal coordinates ($\mathbf{x}^{(j)} \in \mathbb{R}^I$) and values ($\mathbf{u}^{(j)} \in \mathbb{R}^L$). Note that the superscript with parentheses refers to the graph node index. An edge that links node j and k has a feature $\mathbf{e}^{(j,k)}$, which stores indices of segments connected to the edge. For example, when $I = 3$, $L = 2$, node 10 in Figure 1 stores $\mathbf{x}^{(10)} = (x_1^{(10)}, x_2^{(10)}, x_3^{(10)})$ and $\mathbf{u}^{(10)} = (u_1^{(10)}, u_2^{(10)})$. The edge connecting nodes 30 and 12 stores $\mathbf{e}^{(30,12)} = \{5, 7\}$.

A typical message passing in a graph neural network (GNN) returns a hidden state for each graph node which is mostly a tensor (including matrix and vector) [28]. In contrast, INN message passing returns a function (i.e., interpolation function $N^{(j)}(\mathbf{x})$, or often called *shape function* in computational mechanics) for each node ($j = 1, \dots, J$) as a hidden state. In other words, the message passing operation of INN is functional, an operation that returns a function. A general Q -step message passing of INN, $\mathcal{M}^{[q]}(\ast)$, can be expressed as:

$$N^{[q](j)}(\mathbf{x}) = \mathcal{M}^{[q]}(\mathbf{x}^{(j)}, \{\mathbf{x}^{(k)}, \mathbf{e}^{(j,k)} | k \in \mathcal{N}^s(j)\}, N^{[q-1](j)}(\mathbf{x})), \quad q = 1, \dots, Q, \quad N^{[0](j)}(\mathbf{x}) = 0, \quad (1)$$

where $N^{[q](j)}(\mathbf{x})$ is the interpolation function at node j after q -th message passing and $\mathcal{N}^s(j)$ is a set of neighboring nodes of the center node j with s connections (i.e., s -hops, see Supplementary Information for visual illustrations). The operation $\mathcal{M}^{[q](*)}$ constructs an interpolation function $N^{[q](j)}(\mathbf{x})$ for a graph node $\mathbf{x}^{(j)}$ using neighboring nodal coordinates and edge information: $\mathbf{x}^{(k)}, \mathbf{e}^{(j,k)}$. This operation can be any interpolation method such as Lagrange polynomials [29, 22], meshfree [30, 31, 32], and splines [33, 34]. The Q -step message passing implies that it is also possible to progressively construct nonlinear or more problem-specific interpolation functions, theoretically based on the generalized finite element method [35, 36] and convolution hierarchical deep learning neural networks (C-HiDeNN) [7, 18]. Depending on the choice of interpolation technique, other hyper-parameters can be involved in $\mathcal{M}^{[q](*)}$ such as the activation (or basis) function and dilation parameter [7, 18]. See Supplementary Information for various choices of the message passing operation.

During the forward propagation, an input variable $\mathbf{x} \in \mathbb{R}^I$ enters each graph node's interpolation function $N^{[Q](j)}(\mathbf{x})$, followed by a graph-level readout operation:

$$\mathcal{J}\mathbf{u}(\mathbf{x}) = \sum_{j=1}^J N^{(j)}(\mathbf{x})\mathbf{u}^{(j)}, \quad \mathbf{x} \in \mathbb{R}^I, \mathbf{u} \in \mathbb{R}^L. \quad (2)$$

Here, the superscript $[Q]$ is dropped for brevity (i.e., $N^{[Q](j)}(\mathbf{x}) = N^{(j)}(\mathbf{x})$). The interpolation operator \mathcal{J} will designate an interpolated field output throughout this paper. The readout operation can be written as a tensor contraction (or matrix multiplication):

$$\mathcal{J}\mathbf{u}(\mathbf{x}) = \begin{bmatrix} \mathbf{u}^{(1)} & \mathbf{u}^{(2)} & \dots & \mathbf{u}^{(J)} \end{bmatrix} \cdot \begin{bmatrix} N^{(1)}(\mathbf{x}) \\ N^{(2)}(\mathbf{x}) \\ \vdots \\ N^{(J)}(\mathbf{x}) \end{bmatrix} = \mathbf{U}^T \times_2^1 \mathcal{X}(\mathbf{x}) = \mathbf{U}^T \mathcal{X}(\mathbf{x}), \quad (3)$$

where $\mathbf{u}^{(j)} \in \mathbb{R}^L, \mathbf{U} \in \mathbb{R}^{J \times L}, \mathcal{X}(\mathbf{x}) \in \mathbb{R}^J$. The $\mathbf{U}^T \in \mathbb{R}^{L \times J}$ refers to the matrix transpose. Here, $\mathbf{U}^T \times_2^1 \mathcal{X}(\mathbf{x})$ denotes the tensor contraction operation between the second order of tensor \mathbf{U}^T and the first order of tensor $\mathcal{X}(\mathbf{x})$, while $\mathbf{U}^T \mathcal{X}(\mathbf{x})$ is a matrix-vector multiplication. We note that \mathbf{U} is a stack of nodal values $\mathbf{u}^{(j)}$, while $\mathcal{X}(\mathbf{x})$ is a function of \mathbf{x} that is parameterized with nodal coordinates $\mathbf{x}^{(j)}$ in the message passing operation.

The graph node features (i.e., coordinate ($\mathbf{x}^{(j)}$) and value ($\mathbf{u}^{(j)}$)) are trainable parameters of INN. If the nodal coordinates ($\mathbf{x}^{(j)}$) are fixed, one can find nodal values ($\mathbf{u}^{(j)}$) without changing the discretization of the input domain. If the nodal coordinates are also updated, the optimization will adjust the domain discretization similar to the r-adaptivity in FEM [23]. Once the forward propagation is defined, the loss function is chosen based on the problem type: training, solving, and calibration.

Special case 1: regular mesh with Tucker decomposition

When the input domain is discretized with a regular mesh, we can significantly reduce the trainable parameters (or degrees of freedom, DoFs) by leveraging Tensor Decomposition (TD) [16]. One of the widely used TD methods is the Tucker decomposition [37, 38]. Consider a three-input ($I = 3$) and one output ($L = 1$) system and assume the input domain is discretized with $J = J_1 \times J_2 \times J_3$ nodes, as shown in the special case box of Figure 1. To facilitate tensor notation, the nodal values \mathbf{u} will be denoted with left/right super/sub scripts, ${}^m_i \mathbf{u}_l^{(j)}$, where $i \in \mathbb{N}^I$ is the input index, $m \in \mathbb{N}^{M_i}$ is the mode index, $l \in \mathbb{N}^L$ is the output index and $j \in \mathbb{N}^{J_i}$ is the nodal index.

The interpolated field $\mathcal{J}\mathbf{u}(\mathbf{x}) \in \mathbb{R}^{L=1}$ can be represented as a Tucker product:

$$\mathcal{J}\mathbf{u}(\mathbf{x}) = \llbracket \mathcal{G}; (\mathcal{J}_1 \mathbf{u})^T, (\mathcal{J}_2 \mathbf{u})^T, (\mathcal{J}_3 \mathbf{u})^T \rrbracket = \mathcal{G} \times_1^2 (\mathcal{J}_1 \mathbf{u})^T \times_2^2 (\mathcal{J}_2 \mathbf{u})^T \times_3^2 (\mathcal{J}_3 \mathbf{u})^T, \quad (4)$$

where the core tensor $\mathcal{G} \in \mathbb{R}^{M_1 \times M_2 \times M_3}$ is a full trainable matrix typically smaller than the original nodal discretization ($M_1 < J_1, M_2 < J_2, M_3 < J_3$). This enables data compression. The $\mathcal{J}_i \mathbf{u}(x_i) \in \mathbb{R}^{M_i \times 1}$ is the 1-dimensional (1D) interpolated output of i -th input dimension over M_i modes represented as:

$$\mathcal{J} \mathbf{u}(x_i) = \begin{bmatrix} \frac{1}{i} \mathbf{u}^{(1)} & \frac{1}{i} \mathbf{u}^{(2)} & \dots & \frac{1}{i} \mathbf{u}^{(J_i)} \\ \frac{2}{i} \mathbf{u}^{(1)} & \frac{2}{i} \mathbf{u}^{(2)} & \dots & \frac{2}{i} \mathbf{u}^{(J_i)} \\ \vdots & \vdots & \vdots & \vdots \\ M_i \mathbf{u}^{(1)} & M_i \mathbf{u}^{(2)} & \dots & M_i \mathbf{u}^{(J_i)} \end{bmatrix} \cdot \begin{bmatrix} N^{(1)}(x_i) \\ N^{(2)}(x_i) \\ \vdots \\ N^{(J_i)}(x_i) \end{bmatrix} = {}_i \mathbf{U} \times \frac{1}{i} \mathbf{X}(\mathbf{x}) = {}_i \mathbf{U} \mathbf{X}(\mathbf{x}), \quad (5)$$

where ${}_i \mathbf{U} \in \mathbb{R}^{M_i \times J_i}$ and ${}_i \mathbf{X}(\mathbf{x}) \in \mathbb{R}^{J_i \times 1}$. When there is more than one output ($L > 1$), the interpolated field becomes a vector of L elements:

$$\begin{aligned} \mathcal{J} \mathbf{u}(\mathbf{x}) &= [\mathcal{J} u_1(\mathbf{x}), \mathcal{J} u_2(\mathbf{x}), \dots, \mathcal{J} u_L(\mathbf{x})], \text{ where} \\ \mathcal{J} u_l(\mathbf{x}) &= \llbracket \mathcal{G}_l; (\mathcal{J}_1 \mathbf{u}_l)^T, (\mathcal{J}_2 \mathbf{u}_l)^T, (\mathcal{J}_3 \mathbf{u}_l)^T \rrbracket = \mathcal{G}_l \times_1^2 (\mathcal{J}_1 \mathbf{u}_l)^T \times_2^2 (\mathcal{J}_2 \mathbf{u}_l)^T \times_3^2 (\mathcal{J}_3 \mathbf{u}_l)^T. \end{aligned} \quad (6)$$

Special case 2: regular mesh with CP decomposition

Tucker decomposition can be further simplified to CANDECOMP/PARAFAC (CP) decomposition [39, 40, 41] by setting the core tensor \mathcal{G} as an order- I super diagonal tensor: $\mathcal{G} \in \mathbb{R}^{M^I}$, $M = M_1 = \dots = M_I$, all zero entries except the diagonal elements. If we further set the diagonal elements of \mathcal{G} to be 1, the CP decomposition yields:

$$\mathcal{J} \mathbf{u}(\mathbf{x}) = \llbracket \mathcal{G}; (\mathcal{J}_1 \mathbf{u})^T, (\mathcal{J}_2 \mathbf{u})^T, (\mathcal{J}_3 \mathbf{u})^T \rrbracket = \sum_{m=1}^M \prod_{i=1}^I \mathcal{J}^m u(x_i), \quad (7)$$

an inner product of the three interpolated vectors of length M .

It is important to note that the interpolation function $N^{(j)}(x_i)$ in Eq.5 is a one-dimensional function. In other words, both Tucker and CP decomposition replace a high-dimensional interpolation with multiple one-dimensional interpolations that dramatically reduce the number of trainable parameters (or DoFs). As given in Table 1, the number of trainable parameters of the full interpolation scales exponentially with the discretization J_i , whereas the Tucker and the CP decomposition scale linearly with J_i .

Table 1: Number of trainable parameters (or degrees of freedom, DoFs) of full interpolation, Tucker decomposition, and CP decomposition for an I -input single output relationship. The input domain is discretized with a regular grid of $J_1 \times J_2 \times \dots \times J_I$ discretization. Assume that the nodal coordinates (\mathbf{x}^j) are fixed.

	Full interpolation	Tucker decomposition	CP decomposition
Trainable parameters	$\prod_i J_i$	$\prod_i M_i + \sum_i M_i J_i$	$M \sum_i J_i$

INN trainer

A general INN forward propagation is provided in Eq.3 as a tensor contraction. The INN trainer optimizes nodal values $\mathbf{U} = \{\mathbf{u}^{(j)}\}_{j=1, \dots, J}$ (and if needed, nodal coordinates ($\mathbf{X} = \{\mathbf{x}^{(j)}\}_{j=1, \dots, J}$)) under a given loss function and training data. Consider a regression problem with K labeled data: $(\mathbf{x}_k^*, \mathbf{u}_k^*)$, $k = 1, \dots, K$ and $\mathbf{x}_k^* \in \mathbb{R}^I$, $\mathbf{u}_k^* \in \mathbb{R}^L$. Here the superscript * denotes data. A mean squared error (MSE) loss function for this regression problem is defined as:

$$\text{loss}(\mathbf{U}, \mathbf{X}) = \frac{1}{K} \sum_k (\mathcal{J} \mathbf{u}(\mathbf{x}_k^*) - \mathbf{u}_k^*)^2. \quad (8)$$

Finally, an optimization problem is formulated as:

$$\underset{\mathbf{U}, \mathbf{X}}{\text{minimize}} \text{loss}(\mathbf{U}, \mathbf{X}). \quad (9)$$

Several benchmark problems are introduced in the Supplementary Information. The superior training accuracy, faster training and inference time, and fewer trainable parameters of the INN trainer are demonstrated.

INN solver

INN solver generalizes classical numerical methods such as FEM and meshfree, as well as the model order reduction methods such as proper generalized decomposition (PGD) [42] and tensor decomposition (TD) [17, 43]. Here, we

introduce a formulation with CP decomposition to solve the generalized space (\mathbf{x}) - time (t) - parameter ($\boldsymbol{\theta}$) PDE, which is prohibitive for most numerical methods and machine learning approaches [42]. Consider a parameterized space-time PDE:

$$\mathcal{L}u(\mathbf{x}, t, \boldsymbol{\theta}) = 0, \quad (10)$$

where \mathcal{L} is the general partial differential operator (can be linear or nonlinear).

The INN solver uses the same neural network structure as the trainer, but the definition of loss function differs since training data is not known before solving the equation. Instead, the loss function is formulated as the weighted summation of the PDE residual [44, 45, 46]. INN approximates the general space (\mathbf{x}) - time (t) - parameter ($\boldsymbol{\theta}$) solution using the CP decomposition format:

$$\begin{aligned} \mathcal{J}u(\mathbf{x}, t, \boldsymbol{\theta}; \mathbf{U}, \mathbf{X}) = & \sum_{m=1}^M [\mathcal{J}_{x_1}^m u(x_1)] \odot \cdots \odot [\mathcal{J}_{x_d}^m u(x_d)] \odot [\mathcal{J}_t^m u(x_t)] \\ & \odot [\mathcal{J}_{\theta_1}^m u(\theta_1)] \odot \cdots \odot [\mathcal{J}_{\theta_k}^m u(\theta_k)]. \end{aligned} \quad (11)$$

where d and k are the spatial dimension and the number of parameters, respectively. The operator \odot refers to the element-wise multiplication. Similar to the trainer, the goal is to find nodal values \mathbf{U} (and nodal coordinates \mathbf{X} , if one wants to adapt the mesh). As a result, INN obtains the space-time-parameter solution by minimizing the loss function:

$$\underset{\mathbf{U}, \mathbf{X}}{\text{minimize}} \int \delta u \cdot \mathcal{L}[\mathcal{J}u(\mathbf{x}, t, \boldsymbol{\theta}; \mathbf{U}, \mathbf{X})] dx dt d\boldsymbol{\theta}. \quad (12)$$

where δu is the weight function and can be defined using Galerkin, Petrov-Galerkin, collocation or quadratic formulation. It should be noted that INN should automatically satisfy Dirichlet and initial conditions. As a result, only weighted sum residual is considered in the loss function Eq. 11. See the Supplementary Information for detailed derivations of the loss function.

In Supplementary Information, a 3D linear elasticity problem is solved with the full interpolation INN and CP decomposition INN, and compared with FEM. Especially the INN with CP decomposition enables a voxel mesh of 10 million cube - 10^{21} grid points, which expands the state-of-the-art FEM limit by order of 10.

INN calibrator

The word calibration in mathematics refers to a reverse process of regression, where a known or measured observation of the output variables (\mathbf{u}^*) is used to predict the corresponding input variables (\mathbf{x}^*). By definition, it is analogous to solving an inverse problem in engineering design. To build a good calibrator, having an accurate forward model is of paramount importance, followed by building a good optimizer for the inverse problem. A trained or solved INN has the potential to be a superior candidate for the forward model inside a calibrator because it is fully differentiable and accurate, equipped with fast inference time (\sim milliseconds). A general formulation of the INN calibrator is described below:

$$\mathbf{x}^* = \underset{\mathbf{x}}{\text{argmin}} \frac{1}{K} \sum_k (\mathcal{J}u(\mathbf{x}) - \mathbf{u}_k^*)^2, \quad (13)$$

where $\mathcal{J}u(\mathbf{x})$ is the trained or solved forward model, \mathbf{u}_k^* is the k -th measured observation and \mathbf{x}^* is the calibrated input variable.

A few calibration benchmarks are provided in Supplementary Information that demonstrate the superior calibration accuracy and reliability of the INN calibrator.

3 Scientific and Engineering applications

This section will illustrate how Engineering Software 2.0 enabled with INN can be applied to model various facets of metal additive manufacturing by integrating training, solving, and calibration processes. Note that the INN with CP decomposition will be referred to INN for brevity. Laser powder bed fusion (L-PBF) is a type of metal additive manufacturing in which metal powders are layered and melted by a laser beam to create objects that match the

Category	Description	Input/output	Results	
			Visualization	Remarks
Calibration	Heat source parameter calibration $Q^{in}(\mathbf{x}, t, \mathbf{p}) = \frac{2P\eta}{\pi r_b^2 d} e^{-\frac{2(x^2+y^2)}{r_b^2}}$	Depth, $d = p_1 \frac{P}{V} RHF^2$ Absorptivity, $\eta = p_2 \frac{P}{V} RHF^2$ Laser beam radius, $r_b = p_3 \frac{P}{V} RHF^2$		<ul style="list-style-type: none"> only requires 44 simulations INN calibration accuracy = 7.9% MLP does not learn physics given such scarce data
Solving	High-dimensional governing equation for L-PBF $\frac{\partial T(\mathbf{x}, t)}{\partial t} - k\Delta T(\mathbf{x}, t) = S_h(\mathbf{x}, y, P, \eta, d)$	Space-time-parameter inputs (8)/Thermal field		<ul style="list-style-type: none"> Capable of solving number of space-time-parameter grid points up to 3×10^{32} 1.7×10^{25} times less storage requirement compared to FEM.
Training	Real-time online monitoring of L-PBF process	21 Mechanistic features, thermal field, current laser power (input)/laser power required for the next layer		<ul style="list-style-type: none"> 18 to 31 times faster training than MLP. Requires 82% less trainable parameters than MLP. More accurate prediction than MLP.

Figure 2: A summary of engineering applications of the INN methods to scientific and engineering problems. The calibration problem develops a reduced-order model of laser powder bed additive manufacturing to calibrate the heat source parameters from experimental data. A space-time-parameter solution of the same problem with large parameter space is demonstrated in *Solving* category. INN solvers result in significant storage reduction and fast simulation. Finally, a data-driven real-time online monitoring and feedback control tool is formulated with INN that uses only 18% training parameters and is 18-31 times faster compared to MLP.

provided CAD designs [47]. The added flexibility of L-PBF comes with a very large design space and spatially varying microstructure after manufacturing. Therefore, considerable research is being devoted to employing in situ monitoring data for real-time control of L-PBF processes to minimize the variability [8]. Computational modeling of L-PBF spans the simulation of the manufacturing process with a high dimensional design space (solving), computing the internal relationship among different manufacturing parameters (calibrating), and designing an online monitoring and control system for L-PBF (training).

The governing equation for modeling the manufacturing process is given by

$$\frac{\partial T(\mathbf{x}, t)}{\partial t} - k\Delta T(\mathbf{x}, t) = Q_h(\mathbf{x}, t, P, R, \eta, d) \quad (14)$$

This is a heat conduction equation where the moving laser heat source is incorporated through the source term, Q_h . The equation involves spatial parameter \mathbf{x} , temporal variable t , thermal conductivity k , power P , beam radius R , absorptivity η , and laser depth d . For the simplest case of single track laser pass, the initial condition is $T(\mathbf{x}, 0) = T_0(\mathbf{x})$, and the boundary conditions (BC) are $T = \tilde{T}$ in $\partial\Omega_T$ for Dirichlet BC and $\frac{\partial T}{\partial \mathbf{x}} \cdot \mathbf{n} = \bar{q}$ in $\partial\Omega_q$ for Neumann BC, where the spatial domain boundary $\partial\Omega = \partial\Omega_T \cup \partial\Omega_q$.

3.1 Calibration of Heat Source Parameters for Additive Manufacturing

In this example, the INN is used for calibrating a model of heat source of L-PBF, which uses a laser heat source to selectively melt metal powder bed to form a connected shape. A commonly used Gaussian beam profile can be modeled as a volumetric heat source [48]. The heat source equation reads,

$$Q_h(\mathbf{x}, t, \mathbf{p}) = \frac{2P\eta}{\pi r_b^2 d} e^{-\frac{2(x^2+y^2)}{r_b^2}} \quad (15)$$

where, $z_{top} - z \leq d$, z_{top} is z coordinate of the current powder bed surface. The notations follow Eq. 14 and r_b is the standard deviation of the Gaussian source. To get an accurate representation of the physics behind it, model parameters need to be calibrated against experimental data. Following [49], three calibration parameters p_1 , p_2 , and p_3 can be defined as, $d = p_1 \frac{P}{V} RHF^2$, $\eta = p_2 \frac{P}{V} RHF^2$, and $r_b = p_3 \frac{P}{V} RHF^2$. Here, P is laser power, V is the scan speed, and RHF is a residual heat measure predetermined based on a laser toolpath. The challenges for calibrating these parameters are: 1) the computational models are often very expensive to perform even one forward run, 2) the computational models are not automatically differentiable, and 3) limited experimental data is available. As a demonstration for this problem, INN with 1760 trainable parameters is trained on 44 sets of meltpool temperature data generated by the finite difference method (FDM) using 4 different power-scanning speed setup. Later, this trained INN is used for optimizing the three aforementioned parameters using gradient-based optimizers. To show the superiority of INN over traditional neural networks in such data-scarce applications, a 3-layer MLP with 2689 trainable parameters is trained using the same data fed to INN. Details regarding this calibration process are provided in the Supplementary Information.

Both INN-based and MLP-based calibrations are repeated 50 times to give a statistical comparison (see Figure 2). Even with only 44 sets of simulation data, the INN calibrated parameters that produce mean meltpool temperature (or TEP, thermal emission plank) within 7.9% of the experimental data. On the contrary, MLP produced a difference of 44.1% against experimental data, which shows that it hardly learns the underlying physics using such small data with even more trainable parameters.

3.2 Solving High Dimensional Space-Time-Parameter Heat Equation

The governing equation Eq.14 has 8 input variables; 3 for spatial domain (x, y, z), 1 for time domain (t), and 4 for parametric domain (k, p, e, d). See Supplementary Information for a detailed problem definition. This equation is not feasible for process design with most existing computational methods, including the data-driven method inspired by the finite element method (FEM) and the physics-informed neural network (PINN) [20].

To solve the problem with FEM-based data-driven method, one first needs to sample from the 4-dimensional parametric domain, followed by running the time-stepping-based finite element analysis for each sampled parameter set. Then the FEM solutions should be stored as offline training data, and a neural network surrogate model is trained using the data. The computational cost for such operations is prohibitive since large space-time mesh is required in each simulation for real engineering application, as detailed in the Supplementary Information. Moreover, as a larger number of training data is generated due to the high dimensionality of the input domain, this method becomes impractical in terms of data storage. Furthermore, running a large-scale FEM simulation requires a large amount of computational memory.

PINN is a unified framework of training and solving for such parameterized PDEs; however, the computational cost still grows exponentially as the number of input variables grows. As illustrated in Supplementary Information, it is very challenging to solve this 8-dimensional equation. In addition, the convergence of solution accuracy is not guaranteed especially for such high-dimensional problems. Thus, it remains to be seen if PINN can even find a good solution for more than 7 input variables. PINN also suffers from memory issues for GPU training due to the exponential growth of the collocation points although batch training can be adopted to alleviate memory usage.

Contrary to FEM and PINN, INN solves this space-time-parameter problem all-at-once. As it is based on the projected 1D interpolation, the number of trainable parameters increases linearly with the input variables, making the computational cost manageable. Meanwhile, since tensor-decomposed data structures are leveraged, INN has the benefits of significant memory efficiency and storage gain, especially for high-dimensional problems. In Figure 2, we solve the 8-dimensional space-time-parameter PDE with the total number of space-time-parameter grid points of 3×10^{32} , where we use 25,000 grid points to discretize each spatial and parametric coordinate and 50 grid points for the temporal coordinate. The details of the solver example are provided in the Supplementary Information. Since the number of trainable parameters of INN grows linearly, INN has a significant storage gain of 1.7×10^{25} compared to the classical FEM.

Moreover, when using INN, once the parametric solution of the AM problem is obtained, one can easily investigate the uncertainty propagation by imposing probabilistic distributions on the inputs of INN, thanks to the tensor-decomposed data structure. Details on the statistical prediction of parametric solution can be found in the Supplementary Information.

3.3 Real-time Online Control of Laser Powder Bed Fusion Additive Manufacturing

In this application, the INN trainer is used to devise an online control system for L-PBF additive manufacturing. The goal is to maintain a homogeneous melt pool temperature across each layer. The hypothesis is that *a homogeneous melt pool temperature across each layer of material deposition will reduce the variability in the microstructure and mechanical*

properties. The fundamental challenge of implementing a model predictive control system is the computational time required for the forward prediction (involving finite element or computational fluid dynamics models). For prediction, the data is generated by fusing experiments and computational methods (see Supplementary Information for details). The online control loop uses the trained INN model to inform the manufacturing machine. There are two models: *forward model* and *inverse model*.

The forward model uses the mechanistic features (precomputed based on the tool path and geometry of the build to generalize a data-driven model for unseen tool path and geometric features; more details can be found in [50]), and melt pool temperature of the previous layer (measured by the sensor as Thermal Emission Plank (TEP) signal; more details in the Supplementary Information) to predict the TEP/melt pool temperature in the next layer for an uncontrolled process. The uncontrolled TEP is converted to a homogenized TEP over the entire layer. The inverse model takes this targeted, homogenized TEP as the input along with the previous layer’s mechanistic features to predict the required laser power for the next layer. The laser power is then exported to the machine to print the next layer. The forward model is trained on experimentally observed data while the inverse model is trained on computational data coming from a finite element solver. The INN model is applied for both forward and inverse prediction and compared against MLP. Figure 2 shows that for the inverse model INN is at least 18 to 31 times faster to train compared to the MLP to reach the same level of training error, and it uses only about 18% of the parameters that MLP uses. The speed-up depends on the amount of data used. The INN method is consistently more accurate compared to MLP (see Supplementary Information for more details).

4 Conclusions

We show that interpolating neural networks (INN) can train, solve, and calibrate scientific and engineering problems that are extremely challenging or prohibitive for existing numerical methods or machine learning models. The keys to INN’s success in those problems are 1) it interpolates virtual points with well-established interpolation theories (not interpolating training data with a black-box network) and 2) it leverages the idea of separation of variables and tensor decomposition to resolve the curse of dimensionality. Due to the significantly reduced trainable parameters without losing approximation capabilities, INN can train/solve/calibrate faster with less memory requirement, and achieve extremely high model accuracy and fast inference time.

As this is the original article on INN, we have myriads of research questions that may gather huge research interests across various areas including but not limited to scientific machine learning, applied mathematics, computer vision, and data science. To mention a few:

- Multi-resolution aspect (i.e., a varying number of segments across INN networks, M) of INN needs to be investigated. See Supplementary Information for further discussions.
- Convergence of INN for training can be proved mathematically.
- INN training on ensembles of training data might be a way to enhance the generality of the model for image problems or noisy data.
- Since INN could be used as both a solver for physics-based problems and a function approximator for data-driven problems, it is of interest to combine the two behaviors together into one single model, so that we can solve large scale problems involving both complex physics and scarce data. For example, the calibration task of LPBF heat source.

We expect INN can open a next-generation Engineering Software 2.0 by theoretically integrating training, solving, and calibration and tackling extremely challenging problems in the science and engineering domain.

References

- [1] A. Karpathy, Software 2.0 (Mar 2017).
URL <https://karpathy.medium.com/software-2-0-a64152b37c35>
- [2] M. Moor, O. Banerjee, Z. S. H. Abad, H. M. Krumholz, J. Leskovec, E. J. Topol, P. Rajpurkar, Foundation models for generalist medical artificial intelligence, *Nature* 616 (7956) (2023) 259–265.
- [3] A. Vaswani, N. Shazeer, N. Parmar, J. Uszkoreit, L. Jones, A. N. Gomez, Ł. Kaiser, I. Polosukhin, Attention is all you need, *Advances in neural information processing systems* 30 (2017).
- [4] L. Lu, P. Jin, G. Pang, Z. Zhang, G. E. Karniadakis, Learning nonlinear operators via deepnet based on the universal approximation theorem of operators, *Nature machine intelligence* 3 (3) (2021) 218–229.

- [5] C. Zhang, A. Shafieezadeh, Simulation-free reliability analysis with active learning and physics-informed neural network, *Reliability Engineering & System Safety* 226 (2022) 108716.
- [6] S. Goswami, K. Kontolati, M. D. Shields, G. E. Karniadakis, Deep transfer operator learning for partial differential equations under conditional shift, *Nature Machine Intelligence* 4 (12) (2022) 1155–1164.
- [7] C. Park, Y. Lu, S. Saha, T. Xue, J. Guo, S. Mojumder, D. W. Apley, G. J. Wagner, W. K. Liu, Convolution hierarchical deep-learning neural network (c-hidenn) with graphics processing unit (gpu) acceleration, *Computational Mechanics* (2023) 1–27.
- [8] Y. Cai, J. Xiong, H. Chen, G. Zhang, A review of in-situ monitoring and process control system in metal-based laser additive manufacturing, *Journal of Manufacturing Systems* 70 (2023) 309–326.
- [9] G. Leopold, Aws to offer nvidia’s t4 gpus for ai inferencing (Mar 2019).
URL <https://www.hpcwire.com/2019/03/19/aws-upgrades-its-gpu-backed-ai-inference-platform/>
- [10] J. Barr, Amazon ec2 update – inf1 instances with aws inferentia chips for high performance cost-effective inferencing (Dec 2019).
URL <https://aws.amazon.com/blogs/aws/amazon-ec2-update-inf1-instances-with-aws-inferentia-chips-for->
- [11] A. Brohan, N. Brown, J. Carbajal, Y. Chebotar, J. Dabis, C. Finn, K. Gopalakrishnan, K. Hausman, A. Herzog, J. Hsu, et al., Rt-1: Robotics transformer for real-world control at scale, arXiv preprint arXiv:2212.06817 (2022).
- [12] S. Dhar, J. Guo, J. Liu, S. Tripathi, U. Kurup, M. Shah, A survey of on-device machine learning: An algorithms and learning theory perspective, *ACM Transactions on Internet of Things* 2 (3) (2021) 1–49.
- [13] E. Li, L. Zeng, Z. Zhou, X. Chen, Edge ai: On-demand accelerating deep neural network inference via edge computing, *IEEE Transactions on Wireless Communications* 19 (1) (2019) 447–457.
- [14] L. G. Wright, T. Onodera, M. M. Stein, T. Wang, D. T. Schachter, Z. Hu, P. L. McMahon, Deep physical neural networks trained with backpropagation, *Nature* 601 (7894) (2022) 549–555.
- [15] A. Momeni, B. Rahmani, M. Malléjac, P. Del Hougne, R. Fleury, Backpropagation-free training of deep physical neural networks, *Science* 382 (6676) (2023) 1297–1303.
- [16] T. G. Kolda, B. W. Bader, Tensor decompositions and applications, *SIAM review* 51 (3) (2009) 455–500.
- [17] L. Zhang, Y. Lu, S. Tang, W. K. Liu, Hidenn-td: Reduced-order hierarchical deep learning neural networks, *Computer Methods in Applied Mechanics and Engineering* 389 (2022) 114414.
- [18] Y. Lu, H. Li, L. Zhang, C. Park, S. Mojumder, S. Knapik, Z. Sang, S. Tang, D. W. Apley, G. J. Wagner, et al., Convolution hierarchical deep-learning neural networks (c-hidenn): finite elements, isogeometric analysis, tensor decomposition, and beyond, *Computational Mechanics* (2023) 1–30.
- [19] H. Li, S. Knapik, Y. Li, C. Park, J. Guo, S. Mojumder, Y. Lu, W. Chen, D. W. Apley, W. K. Liu, Convolution hierarchical deep-learning neural network tensor decomposition (c-hidenn-td) for high-resolution topology optimization, *Computational Mechanics* (2023) 1–20.
- [20] M. Raissi, P. Perdikaris, G. E. Karniadakis, Physics-informed neural networks: A deep learning framework for solving forward and inverse problems involving nonlinear partial differential equations, *Journal of Computational physics* 378 (2019) 686–707.
- [21] Y. LeCun, Y. Bengio, et al., Convolutional networks for images, speech, and time series, *The handbook of brain theory and neural networks* 3361 (10) (1995) 1995.
- [22] W. K. Liu, S. Li, H. S. Park, Eighty years of the finite element method: Birth, evolution, and future, *Archives of Computational Methods in Engineering* 29 (6) (2022) 4431–4453.
- [23] L. Zhang, L. Cheng, H. Li, J. Gao, C. Yu, R. Domel, Y. Yang, S. Tang, W. K. Liu, Hierarchical deep-learning neural networks: finite elements and beyond, *Computational Mechanics* 67 (2021) 207–230.
- [24] S. Saha, Z. Gan, L. Cheng, J. Gao, O. L. Kafka, X. Xie, H. Li, M. Tajdari, H. A. Kim, W. K. Liu, Hierarchical deep learning neural network (hidenn): An artificial intelligence (ai) framework for computational science and engineering, *Computer Methods in Applied Mechanics and Engineering* 373 (2021) 113452.
- [25] F. Alet, A. K. Jeewajee, M. B. Villalonga, A. Rodriguez, T. Lozano-Perez, L. Kaelbling, Graph element networks: adaptive, structured computation and memory, in: *International Conference on Machine Learning*, PMLR, 2019, pp. 212–222.
- [26] M. Y. Michelis, R. K. Katzschmann, Physics-constrained unsupervised learning of partial differential equations using meshes, arXiv preprint arXiv:2203.16628 (2022).

- [27] H. Gao, M. J. Zahr, J.-X. Wang, Physics-informed graph neural galerkin networks: A unified framework for solving pde-governed forward and inverse problems, *Computer Methods in Applied Mechanics and Engineering* 390 (2022) 114502.
- [28] Z. Wu, S. Pan, F. Chen, G. Long, C. Zhang, S. Y. Philip, A comprehensive survey on graph neural networks, *IEEE transactions on neural networks and learning systems* 32 (1) (2020) 4–24.
- [29] T. J. Hughes, *The finite element method: linear static and dynamic finite element analysis*, Courier Corporation, 2003.
- [30] W. K. Liu, S. Jun, Y. F. Zhang, Reproducing kernel particle methods, *International journal for numerical methods in fluids* 20 (8-9) (1995) 1081–1106.
- [31] T. Belytschko, Y. Y. Lu, L. Gu, Element-free galerkin methods, *International journal for numerical methods in engineering* 37 (2) (1994) 229–256.
- [32] G.-R. Liu, Y.-T. Gu, *An introduction to meshfree methods and their programming*, Springer Science & Business Media, 2005.
- [33] L. Schumaker, *Spline functions: basic theory*, Cambridge university press, 2007.
- [34] T. J. Hughes, J. A. Cottrell, Y. Bazilevs, Isogeometric analysis: Cad, finite elements, nurbs, exact geometry and mesh refinement, *Computer methods in applied mechanics and engineering* 194 (39-41) (2005) 4135–4195.
- [35] T. Strouboulis, K. Copps, I. Babuška, The generalized finite element method, *Computer methods in applied mechanics and engineering* 190 (32-33) (2001) 4081–4193.
- [36] R. Tian, Extra-dof-free and linearly independent enrichments in gfem, *Computer Methods in Applied Mechanics and Engineering* 266 (2013) 1–22.
- [37] L. R. Tucker, Implications of factor analysis of three-way matrices for measurement of change, *Problems in measuring change* 15 (122-137) (1963) 3.
- [38] L. R. Tucker, Some mathematical notes on three-mode factor analysis, *Psychometrika* 31 (3) (1966) 279–311.
- [39] R. A. Harshman, et al., Foundations of the parafac procedure: Models and conditions for an “explanatory” multi-modal factor analysis, *UCLA working papers in phonetics* 16 (1) (1970) 84.
- [40] J. D. Carroll, J.-J. Chang, Analysis of individual differences in multidimensional scaling via an n-way generalization of “eckart-young” decomposition, *Psychometrika* 35 (3) (1970) 283–319.
- [41] H. A. Kiers, Towards a standardized notation and terminology in multiway analysis, *Journal of Chemometrics: A Journal of the Chemometrics Society* 14 (3) (2000) 105–122.
- [42] F. Chinesta, P. Ladeveze, E. Cueto, A short review on model order reduction based on proper generalized decomposition, *Archives of Computational Methods in Engineering* 18 (4) (2011) 395–404.
- [43] J. Guo, C. Park, X. Xie, Z. Sang, G. J. Wagner, W. K. Liu, Convolutional hierarchical deep learning neural networks-tensor decomposition (c-hidenn-td): a scalable surrogate modeling approach for large-scale physical systems, *arXiv preprint arXiv:2409.00329* (2024).
- [44] E. Pruliere, F. Chinesta, A. Ammar, On the deterministic solution of multidimensional parametric models using the proper generalized decomposition, *Mathematics and Computers in Simulation* 81 (4) (2010) 791–810.
- [45] E. Kharazmi, Z. Zhang, G. E. Karniadakis, Variational physics-informed neural networks for solving partial differential equations, *arXiv preprint arXiv:1912.00873* (2019).
- [46] E. Kharazmi, Z. Zhang, G. E. Karniadakis, hp-vpinns: Variational physics-informed neural networks with domain decomposition, *Computer Methods in Applied Mechanics and Engineering* 374 (2021) 113547.
- [47] V. Bhavar, P. Kattire, V. Patil, S. Khot, K. Gujar, R. Singh, A review on powder bed fusion technology of metal additive manufacturing, *Additive manufacturing handbook* (2017) 251–253.
- [48] Y. Li, S. Mojumder, Y. Lu, A. A. Amin, J. Guo, X. Xie, W. Chen, G. J. Wagner, J. Cao, W. K. Liu, Statistical parameterized physics-based machine learning digital twin models for laser powder bed fusion process, *arXiv preprint arXiv:2311.07821* (2023).
- [49] A. A. Amin, Y. Li, Y. Lu, X. Xie, Z. Gan, S. Mojumder, G. J. Wagner, W. K. Liu, Physics guided heat source for quantitative prediction of in718 laser additive manufacturing processes, *npj Computational Materials* 10 (37) (2024).
- [50] D. Kozjek, F. M. Carter III, C. Porter, J.-E. Mogonye, K. Ehmann, J. Cao, Data-driven prediction of next-layer melt pool temperatures in laser powder bed fusion based on co-axial high-resolution planck thermometry measurements, *Journal of Manufacturing Processes* 79 (2022) 81–90.